REVIEWS

Journal of Semiconductors
(2019) 40, 101306
doi: 10.1088/1674-4926/40/10/101306

Dynamics of InAs/GaAs quantum dot lasers epitaxially grown on Ge or Si substrate

Cheng Wang[1, †] and Yueguang Zhou[1, 2, 3]

[1]School of Information Science and Technology, ShanghaiTech University, Shanghai 201210, China

[2]Shanghai Institute of Microsystem and Information Technology, Chinese Academy of Sciences, Shanghai 200050, China

[3]University of Chinese Academy of Sciences, Beijing 100049, China

Abstract: Growing semiconductor laser sources on silicon is a crucial but challenging technology for developing photonic integrated circuits (PICs). InAs/GaAs quantum dot (Qdot) lasers have successfully circumvented the mismatch problem between III–V materials and Ge or Si, and have demonstrated efficient laser emission. In this paper, we review dynamical characteristics of Qdot lasers epitaxially grown on Ge or Si, in comparison with those of Qdot lasers on native GaAs substrate. We discuss properties of linewidth broadening factor, laser noise and its sensitivity to optical feedback, intensity modulation, as well as mode locking operation. The investigation of these dynamical characteristics is beneficial for guiding the design of PICs in optical communications and optical computations.

Key words: quantum dot laser; laser noise; modulation dynamics; mode locking; photonic integrated circuits

Citation: C Wang and Y G Zhou, Dynamics of InAs/GaAs quantum dot lasers epitaxially grown on Ge or Si substrate[J]. *J. Semicond.*, 2019, 40(10), 101306. http://doi.org/10.1088/1674-4926/40/10/101306

1. Introduction

High-speed optical communication and fast neuromorphic optical computation highly demand low-cost photonic integrated circuits (PIC) on the silicon platform[1, 2]. A large variety of photonic devices on Si have been demonstrated, including optical waveguides, optical modulators, photodiodes, and laser sources[3–6]. Among these devices, it is the most challenging to integrate III–V semiconductor lasers on Si. On one hand, Si is nonpolar material while III–V compound is polar material, and hence the monolithic integration results in antiphase boundaries[7]. On the other hand, the lattice mismatch between Si and III–V compound leads to high density of threading dislocations[8]. Both defects induce significant nonradiative recombination of carriers and thus hinder efficient radiative recombination for laser emission. Instead of monolithic integration, flip-chip bonding and wafer bonding provide alternative approaches for integration of semiconductor lasers on Si[9–11]. These two methods are less challenging but the yield is low and the cost is high. Thanks to the individual nature of quantum dots (Qdot), Qdots are more tolerant to epitaxial defects than quantum well (Qwell) structures, and hence permit efficient stimulated emission in the presence of high-density defects[12–14]. In addition, Qdot lasers have shown superior performances over conventional Qwell lasers, including low threshold current density, high temperature stability, strong resistance to residual optical feedback and so on[15–17]. Consequently, III–V Qdot lasers become the primary choice for monolithic integrated laser sources on Si. The first epitaxial integration of InAs/GaAs Qdot lasers operated at room temperature was achieved on Ge substrate rather than Si substrate in 2011[12], because the lattice constant of GaAs was closely matched to Ge (0.08% mismatch). Since then, tremendous works have been done to demonstrate the laser emission of InAs/GaAs Qdot lasers epitaxially grown on Ge-on-Si substrate, offcut Si substrate, and on-axis (001) Si substrate[18–20]. A lot of efforts have been devoted to minimize the defect density through optimization of the buffer layer, and the defect density has been reduced down to the order of 10^6 cm^{-2}, which is yet at least two orders of magnitude higher than that of Qdot laser on the native GaAs substrate[19, 21]. Meanwhile, static performances of Qdot lasers on Ge or Si have shown considerable improvements, in aspects of the threshold current density, the quantum efficiency, the high temperature operation, as well as the aging lifetime[14, 20, 22]. There are a bunch of papers discussing the steady-state characteristics of Ge- or Si-based Qdot lasers, and some review works can refer to references[23–25].

Based on the improvement of static performances, dynamical characteristics of Ge- or Si-based Qdot lasers are drawing more and more attentions, which can directly determine the design of PIC systems. This article provides an overview of recent progresses on the laser dynamics of linewidth broadening factor (LBF), relative intensity noise (RIN), frequency noise (FN, or phase noise), sensitivity to optical feedback, intensity modulation, and mode locking operation, which are compared to those of Qdot lasers grown on native GaAs substrate. The paper is organized as follows: Section 2 introduces a rate equation model for Qdot lasers and analyzes all the dynamical characteristics theoretically. Section 3 discusses the LBF, and Section 4 discusses the RIN and its sensitivity to optical feedback. Section 5 investigates the direct intensity modulation including both the small-signal response and the large-signal response. Section 6 studies the mode lock-

Correspondence to: C Wang, wangcheng1@shanghaitech.edu.cn
Received 23 MAY 2019; Revised 12 JULY 2019.

ing characteristics of Si-based Qdot lasers. Section 7 discusses the future trends, and Section 8 summarizes this work.

2. Rate equation analysis

The rate equation model for Qdot lasers takes into account the carrier dynamics in the carrier reservoir (RS, wetting layer), in the first excited state (ES), and in the ground state (GS). The Qdot laser is assumed to emit solely on a single mode at the GS, and the inhomogeneous broadening effect is not considered. The coupled rate equations for the carrier numbers (N_{RS}, N_{ES}, N_{GS}), the photon number (S), and the phase (φ) of the electric field are given by[26]

$$\frac{dN_{RS}}{dt} = \eta\frac{I}{q} + \frac{N_{ES}}{\tau_{RS}^{ES}} - \frac{N_{RS}}{\tau_{ES}^{RS}}(1-\rho_{ES}) - \frac{N_{RS}}{\tau_{RS}^{spon}} - \frac{N_{RS}}{\tau_{nr}} + F_{RS}, \quad (1)$$

$$\frac{dN_{ES}}{dt} = \left(\frac{N_{RS}}{\tau_{ES}^{RS}} + \frac{N_{GS}}{\tau_{ES}^{GS}}\right)(1-\rho_{ES}) - \frac{N_{ES}}{\tau_{GS}^{ES}}(1-\rho_{GS}) - \frac{N_{ES}}{\tau_{RS}^{ES}} - \frac{N_{ES}}{\tau_{ES}^{spon}} - \frac{N_{ES}}{\tau_{nr}} + F_{ES}, \quad (2)$$

$$\frac{dN_{GS}}{dt} = \frac{N_{ES}}{\tau_{GS}^{ES}}(1-\rho_{GS}) - \frac{N_{GS}}{\tau_{ES}^{GS}}(1-\rho_{ES}) - \Gamma_P v_g g_{GS} S - \frac{N_{GS}}{\tau_{GS}^{spon}} - \frac{N_{GS}}{\tau_{nr}} + F_{GS}, \quad (3)$$

$$\frac{dS}{dt} = \left(\Gamma_p v_g g_{GS} - \frac{1}{\tau_p}\right)S + \beta_{SP}\frac{N_{GS}}{\tau_{GS}^{spon}} + F_S, \quad (4)$$

$$\frac{d\varphi}{dt} = \frac{1}{2}\Gamma_P v_g\left(g_{GS}k_{GS} + g_{ES}k_{ES} + g_{RS}k_{RS}\right) + F_\varphi, \quad (5)$$

where I is the pump current, and η is the current injection efficiency. τ_{ES}^{RS} is the carrier capture time from the RS to the ES, τ_{GS}^{ES} is the carrier relaxation time from the ES to the GS, and τ_{RS}^{ES} and τ_{ES}^{GS} are the corresponding carrier escape times due to thermal excitation. $\tau_{RS,ES,GS}^{spon}$ is the spontaneous emission lifetime, τ_p is the photon lifetime in the cavity, and τ_{nr} is the nonradiative recombination lifetime due to the defect, which is assumed to be the same for all the three carrier states. $\rho_{ES,GS}$ is the carrier occupation probability, and $g_{RS,ES,GS}$ is the material gain. Γ_p is the optical confinement factor, v_g is the group velocity of light, and β_{sp} is the spontaneous emission factor. $k_{RS,ES,GS}$ is a coefficient weighting for the carrier contribution of each state to the LBF at the lasing mode. $F_{RS,ES,GS}$, F_S, and F_φ are Langevin noise sources for the carrier, the photon, and the phase, respectively. The laser dynamics are obtained through the small-signal analysis of the coupled rate equations, and the parameters used for the simulations are listed in Table 1[26].

Epitaxial defect in semiconductors induces nonradiative recombination through the Shockley-Read-Hall process, and the nonradiative recombination lifetime τ_{nr} is inversely proportional to the defect density. The defect density in GaAs-based Qdot lasers is 10^3–10^4 cm^{-2} or less, and the corresponding τ_{nr} is on the order of 10 ns, which is much longer than the spontaneous emission lifetime (~1.0 ns). Therefore, the nonradiative recombination term in the rate equations is negligible[27]. On the other hand, the defect density in Ge- or Si-based Qdot lasers is at least two orders of magnitude higher (10^6–10^8 cm^{-2}) than that in GaAs-based lasers[12, 19]. Therefore, the nonradiative lifetime of Ge- or Si-based lasers can be below 0.1 ns, which becomes shorter than the spontaneous emission lifetime and hence can not be neglected in rate equations. The simulations in this section focus on the impacts of the non-radiative recombination or the defect density on the laser dynamics. The emitted photon number is fixed at 2×10^5 for all the simulations unless stated otherwise.

Table 1. Qdot laser parameters used for the simulation.

Symbol	Description	Value
τ_{ES}^{RS}	RS to ES capture time	6.3 ps
τ_{GS}^{ES}	ES to GS relaxation time	2.9 ps
τ_{RS}^{ES}	ES to RS escape time	2.7 ns
τ_{ES}^{GS}	GS to ES escape time	10.4 ps
τ_{RS}^{spon}	RS spontaneous emission time	0.5 ns
τ_{ES}^{spon}	ES spontaneous emission time	0.5 ns
τ_{GS}^{spon}	GS spontaneous emission time	1.2 ns
τ_p	Photon lifetime	4.1 ps
T_2	Polarization dephasing time	0.1 ps
β_{sp}	Spontaneous emission factor	1.0×10^{-4}
a_{GS}	GS differential gain	5.0×10^{-15} cm^2
a_{ES}	ES differential gain	10×10^{-15} cm^2
a_{RS}	RS differential gain	2.5×10^{-15} cm^2
ξ	Gain compression factor	2.0×10^{-16} cm^3
Γ_p	Optical confinement factor	0.06
a_{GS}	GS contribution to LBF	0.50
N_B	Total dot number	10^7
D_{RS}	Total RS state number	4.8×10^6
V_B	Active region volume	5.0×10^{-11} cm^3
V_{RS}	RS region volume	1.0×10^{-16} cm^3

The simulations in Fig. 1 show that the fast nonradiative recombination process or the high defect density raises the threshold current, which is the same as widely observed in experiments[28, 29]. In addition, carrier populations in the ES and in the RS are raised as well. On the other hand, the carrier population in the GS has no change because of the gain clamping effect[30].

The LBF characterizes the coupling ratio of the carrier-induced refractive index variation to the gain variation in semiconductor lasers[31]. It is a crucial parameter determining the spectral linewidth, the chirp under direct modulation, the nonlinear dynamics behavior like chaos, and so on[27, 32–35]. Typical LBFs of Qwell lasers are in the range of 2.0–5.0, while the LBF of ideal Qdot lasers is expected to be near-zero owing to the delta-function like density of states[36, 37]. However, the reported LBF values of Qdot lasers range from near-zero up to more than 10[38–41], due to the inhomogeneous broadening effect and the influence of the ES[42]. Fig. 2 shows that a

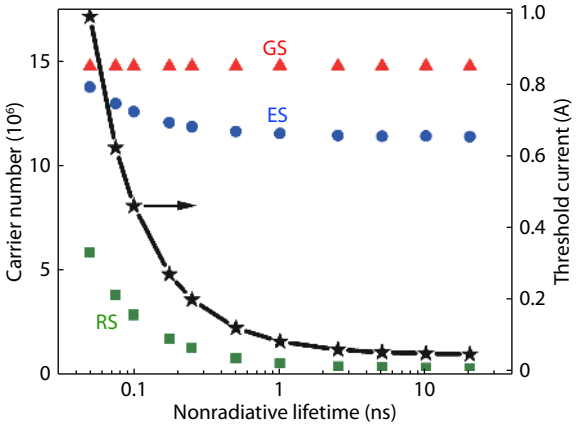

Fig. 1. (Color online) Nonradiative recombination effects on the threshold current and the carrier numbers in GS, ES, and RS at the threshold, respectively.

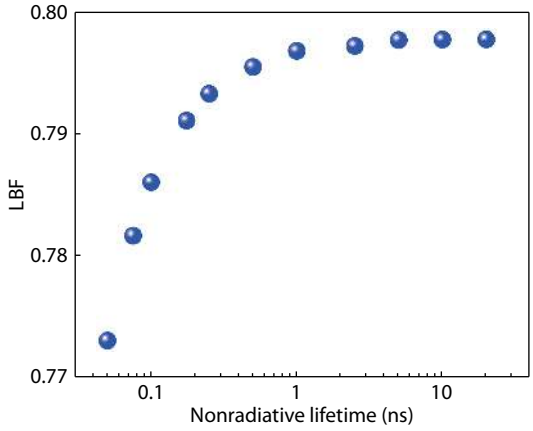

Fig. 2. (Color online) Nonradiative recombination effects on the LBF. (Reproduced from Ref. [43].)

fast nonradiative recombination rate slightly reduces the LBF. This is because a short carrier lifetime is helpful to reduce the LBF of semiconductor lasers[26]. On the other hand, although the fast nonradiative recombination strongly increases the carrier accumulation in the RS, it has little impact on the LBF because the coefficient k_{RS} is small[26].

The RIN characterizes the intensity noise of semiconductor lasers, and it is defined as the ratio of the power spectral density of intensity noise to the square of the averaged optical power[27]. The RIN of semiconductor lasers originates from the intrinsic spontaneous emission noise, the intrinsic carrier noise[44], as well as low-frequency technical noise sources including the current noise of the power source, the temperature fluctuation, and the mechanical vibrations[45, 46]. The Langevin noise sources in rate Eqs. (1)–(5) characterize the intrinsic noise while the technical noise is not included in the model. Fig. 3(a) demonstrates that a short nonradiative recombination lifetime raises the RIN level at low frequencies. Fig. 3(c) shows that the low-frequency RIN increases from −144 dB/Hz at τ_{nr} = 10 ns up to −140 dB/Hz at τ_{nr} = 0.1 ns. The increase of the RIN is attributed to a shorten carrier lifetime induced by high density defects[27, 47].

The FN of semiconductor laser originates from the spontaneous emission as well. The high-frequency (> 20 GHz) FN in Fig. 3(b) determines the Schawlow-Townes linewidth. However, the low-frequency (< 1.0 GHz) FN in Fig. 3(b) is amplified by the LBF (α) by a factor of $(1 + \alpha^2)$, which directly determines the total spectral linewidth of semiconductor lasers[27]. Fig. 3(b) proves that the nonradiative recombination has little impact on either the Schawlow-Townes linewidth or the total spectral linewidth of Qdot lasers. However, the FN resonance peak is significantly suppressed for a short nonradiative recombination lifetime. The amplitude of the peak FN in Fig. 3(c) decreases from 1.40×10^6 Hz^2/Hz at τ_{nr} = 10 ns down to 0.98×10^6 Hz^2/Hz at τ_{nr} = 0.1 ns.

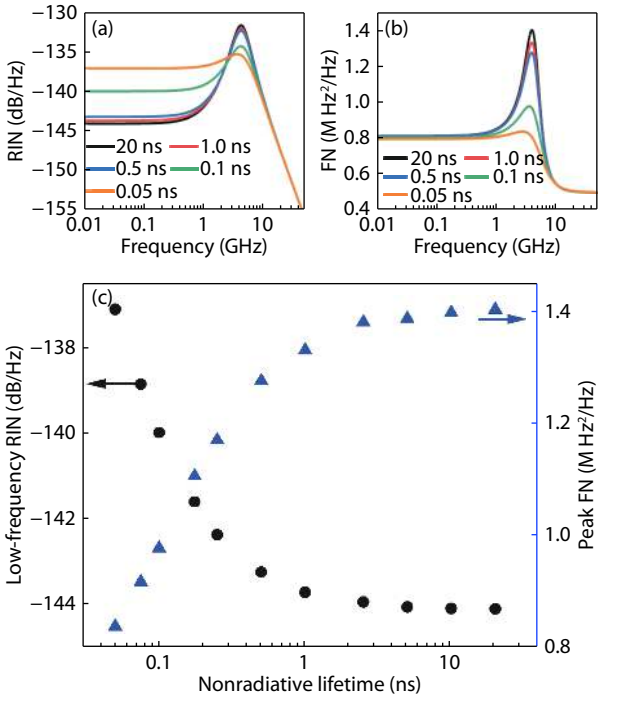

Fig. 3. (Color online) Non-radiative recombination effects on (a) the RIN spectrum, (b) the FN spectrum, and (c) the low-frequency RIN and the peak FN.

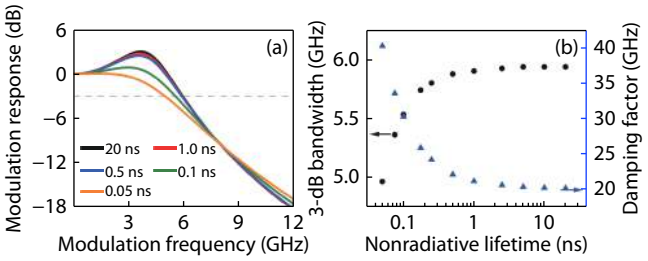

Fig. 4. (Color online) Non-radiative recombination effects on (a) the intensity modulation response, and (b) the 3-dB modulation bandwidth and the damping factor.

Fig. 4(a) shows that the fast nonradiative recombination suppresses the resonance peak. This is because the nonradiative recombination shortens the total carrier lifetime and hence significantly enhances the damping factor in Fig. 4(b). Consequently, the modulation bandwidth in Fig. 4(b) is reduced slightly from 5.9 GHz at τ_{nr} = 10 ns down to 5.5 GHz at τ_{nr} = 0.1 ns.

Semiconductor lasers in an optical system inevitably suffer from residual optical feedback due to optical connectors or other optical devices in the optical link. When the feedback strength reaches a certain level defined as the critical feedback level, the laser becomes oscillating in the chaos state, which is also known as coherence collapse[48]. Both the

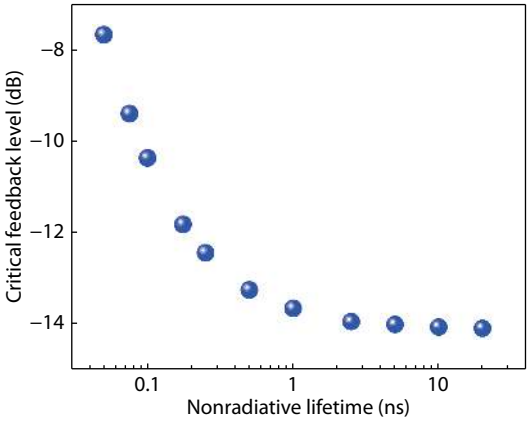

Fig. 5. (Color online) Non-radiative recombination effects on the critical feedback level. (Reproduced from Ref. [43].)

RIN and the FN are significantly raised, and the coherence of the laser becomes extremely poor, which are destructive for optical communication or optical computing. Therefore, an optical isolator is usually packaged together with the semiconductor laser in commercial laser transmitters. In comparison with Qwell lasers, Qdot lasers have shown much stronger tolerance to optical feedback, and the critical feedback level is at least two orders of magnitude higher[15, 49]. This makes Qdot lasers very promising for isolator-free operation in optical links.

There are several analytical models evaluating the critical feedback level of semiconductor lasers[50–52]. One classical formula was proposed by Helms and Petermann[51]:

$$f_{\mathrm{ext,c}} = \frac{\Gamma^2(1+\alpha^2)}{\alpha^4}\frac{\tau_{\mathrm{in}}^2 R}{4(1-R)^2}, \tag{6}$$

where Γ is the damping factor, R is the facet reflectivity, and τ_{in} is the light round-trip time in the laser cavity. According to Eq. (6), a large damping factor and/or a small LBF are desirable for increasing the critical feedback level. Surprisingly, fast nonradiative recombination in Fig. 5 raises the critical feedback level from −14.0 dB at τ_{nr} = 10 ns up to −10.4 dB at τ_{nr} = 0.1 ns. This is understandable because the nonradiative recombination substantially enhances the damping factor in Fig. 4(b), and slightly reduces the LBF in Fig. 2.

3. Linewidth broadening factor

In experiments, the LBF of semiconductor lasers can be measured by a few techniques as reviewed in Ref. [32]. However, the most widely employed method is the Hakki-Paoli method[41, 42], which is based on the optical spectrum analysis of the amplified spontaneous emission when the laser is operated below the lasing threshold. Through measuring the wavelength shift (dλ) and the net modal gain variation (g_{net}) of longitudinal modes with the pump current change (dI), the LBF is determined by

$$\alpha = -\frac{2\pi}{L\Delta\lambda} \times \frac{\mathrm{d}\lambda/\mathrm{d}I}{\mathrm{d}g_{\mathrm{net}}/\mathrm{d}I}, \tag{7}$$

with L being the cavity length, and $\Delta\lambda$ being the adjacent mode spacing. However, the accuracy of this method is limited by the thermal effect, which induces red-shift of the longitudinal mode. Therefore, pulsed power source is usually

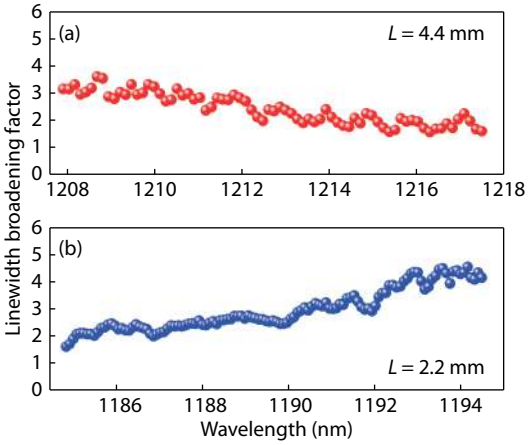

Fig. 6. (Color online) Sub-threshold LBF of Ge-based Qdot lasers with a cavity length of (a) 4.4 mm and (b) 2.2 mm. Both lasers have a ridge width of 4.0 μm, and a lasing threshold of 60 mA.

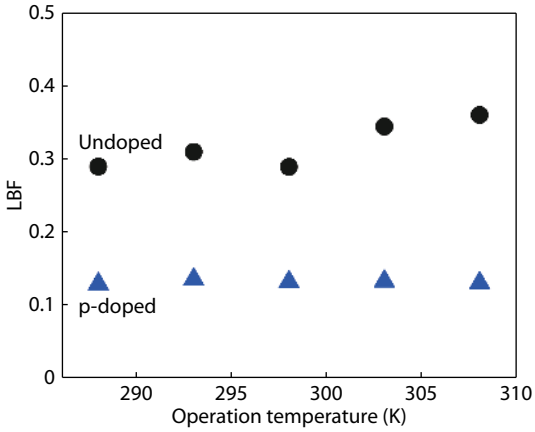

Fig. 7. (Color online) LBFs of Si-based undoped (closed circle) and p-doped (triangle) Qdot lasers. (Reproduced from Ref. [55].)

used to pump the laser to reduce the thermal effect, which in turn weakens the optical signal. In 2016, Wang *et al.* proposed an improved Hakki-Paoli method taking advantage of the optical injection locking technique, which was thermally insensitive and hence improved the accuracy of LBF measurement[53].

Fig. 6 investigates the sub-threshold LBFs of Qdot lasers epitaxially grown on a Ge(100) wafer with 6° off-cut towards [111] plane by the gas-source molecular beam epitaxy based on the Hakki-Paoli method. The active region of the two laser samples consists of five stack layers of dot-in-well structures. Both lasers are fabricated from the same wafer, and are operated on GS. The only difference between the two laser devices is the cavity length. Fig. 6(a) shows that the LBF of the Ge-based laser with a cavity length of 4.4 mm decreases from 3.0 at 1208 nm down to 2.0 at 1218 nm. The LBF at gain peak of 1213 nm is around 2.5. In contrast, Fig. 6(b) shows that the LBF of the Ge-based laser with a cavity length of 2.2 mm increases from 1.7 at 1184 nm up to 4.1 at 1194 nm. The LBF at the gain peak of 1190 nm is about 3.0. The different tendency of the LBF versus the lasing wavelength in both laser can be attributed to the large dot size dispersion[43], which leads to a broad photoluminescence linewidth (full width at half maximum) of 48 meV[54].

Fig. 7 studies sub-threshold LBFs of InAs/GaAs Qdot lasers epitaxially grown on an on-axis Si (001) wafer by the sol-

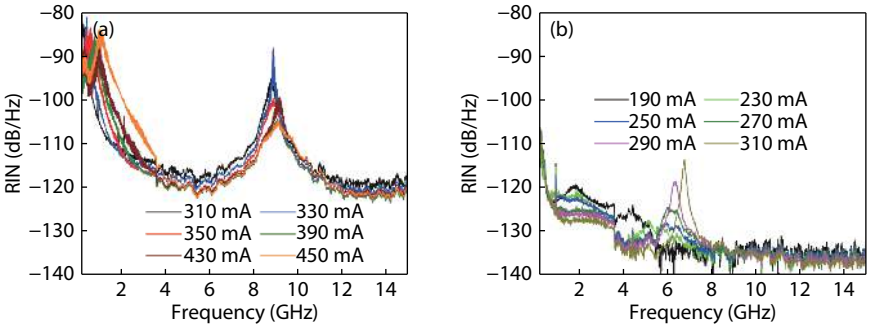

Fig. 8. (Color online) RINs of (a) Ge-based Qdot laser (I_{th} = 300 mA), and (b) GaAs-based Qdot laser (I_{th} = 120 mA). (Reproduced from Ref. [58].)

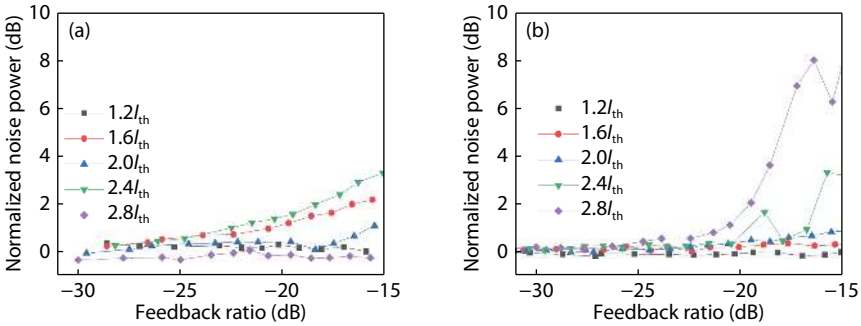

Fig. 9. (Color online) Optical feedback effects on the normalized intensity noise power of (a) Ge-based laser (I_{th} = 75 mA), and (b) GaAs-based laser (I_{th} = 60 mA), with respect to the free-running cases. The noise power is averaged in the frequency range of 10–100 MHz. (Reproduced from Ref. [43].)

id-source molecular beam epitaxy[56]. The active region consists of 4 stack layers of dot-in-well structures. Fig. 7 shows that the undoped laser (closed circle) exhibits a low LBF of 0.31 at the gain peak, when the laser is operated at 293 K. The ultralow LBF is mainly attributed to the low Qdot size dispersion, which exhibits a rather narrow inhomogeneous broadening linewidth of 29 meV in the photoluminescence spectrum. Increasing the operation temperature slightly increases the LBF value of the undoped laser. In contrast, the p-doped laser (triangle) shows a reduced LBF of 0.13, owing to the lower transparency carrier density[57]. Besides, the LBF of the p-doped laser is insensitive to the operation temperature.

It is remarked that although Fig. 2 shows that the nonradiative recombination slightly reduces the LBF, it is negligible in comparison with the inhomogeneous broadening effect[43]. The different dot size dispersion from device to device leads to the wide spread of LBF values from near-zero up to more than 10[39–42]. Therefore, as long as the dot size dispersion is similar, the LBFs of Ge- or Si-based Qdot lasers are expected to be comparable to those of GaAs- or InP-based ones.

4. RIN and sensitivity to optical feedback

Fig. 8 compares the measured RINs of a Ge-based Qdot laser and of a GaAs-based one. Both lasers have the same epilayer structure except the substrate[58]. It is shown that the minimum RIN level of the Ge-based laser is about 15-dB higher than that of the GaAs-based one. This is in consistent with the simulation in Fig. 3(a), and hence the larger RIN in the Ge-based laser is attributed to the higher density of defect (~10^6 cm^{-2}). It is worthwhile to mention that the broad peak around 9.0 GHz in Fig. 8(a) arises from the photon-photon resonance, which is owing to the quasi-phase locking of adjacent longitudinal modes[59, 60]. The detailed analysis of the resonance will be reported elsewhere.

Fig. 9 compares the feedback sensitivity of a Ge-based Qdot laser and a GaAs-based one. Both lasers have the same epilayer structure and the same cavity structure[43]. It is shown that the optical feedback with a feedback ratio of –15 dB raises the noise power of the Ge-based laser in Fig. 9(a) by about 4.0 dB. In contrast, the noise power of the GaAs-based laser in Fig. 9(b) is increased by 8.0 dB. This experimental result is in agreement with the simulation in Fig. 5, and the enhanced feedback tolerance of the Ge-based Qdot laser is mainly attributed to the higher damping factor as described in Fig. 4(b).

Fig. 10 compares the measured RINs of a 1.3 μm InAs/GaAs Qdot laser epitaxially grown on (001)Si and of a 1.5 μm AlGaInAs Qwell laser heterogeneously integrated on Si[61]. It is shown that the RIN of the Qdot laser with very weak feedback (–60 dB) in Fig. 10(a) is about 15 dB higher than that of the Qwell laser in Fig. 10(b), which is again due to the high density defect. However, the RIN of the Qdot laser only slightly increases with increasing feedback level, and does not show any feature of coherence collapse. In contrast, the Qwell laser exhibits a critical feedback level around –30 dB, beyond which the feedback significantly raises the RIN level[62].

The experimental observation in Fig. 10 is confirmed through measuring the optical spectrum and the electrical spectrum in Fig. 11[63]. It is shown that the optical feedback has little effect on both the optical spectrum (Fig. 11(a)) and the electrical spectrum (Fig. 11(c)) of the Si-based Qdot laser up to a feedback ratio of –7.4 dB (100%). In contrast, the Qwell laser loses stability beyond a critical feedback level of –25 dB (1.7%). The optical spectrum (Fig. 11b) is significantly broadened, and the electrical spectrum (Fig. 11(d)) becomes very noisy within a broad bandwidth of 10 GHz. Finally, it is

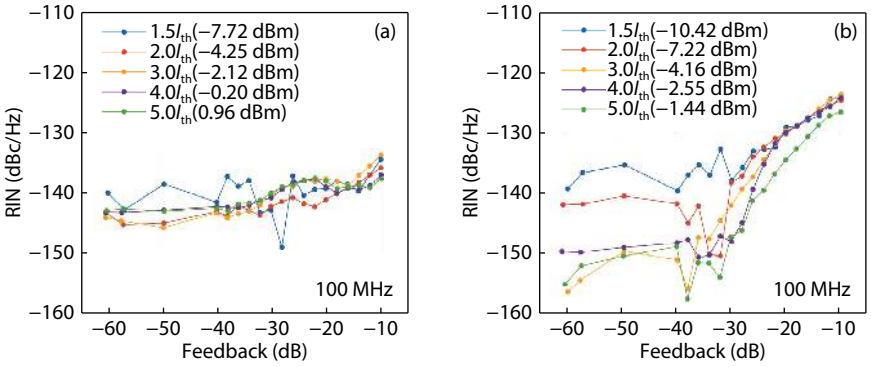

Fig. 10. (Color online) Effects of optical feedback on RINs of (a) a Qdot laser epitaxially grown on Si (I_{th} = 38 mA), and of (b) a Qwell laser heterogeneously integrated on Si (I_{th} = 32 mA). (Reproduced from Ref. [61].)

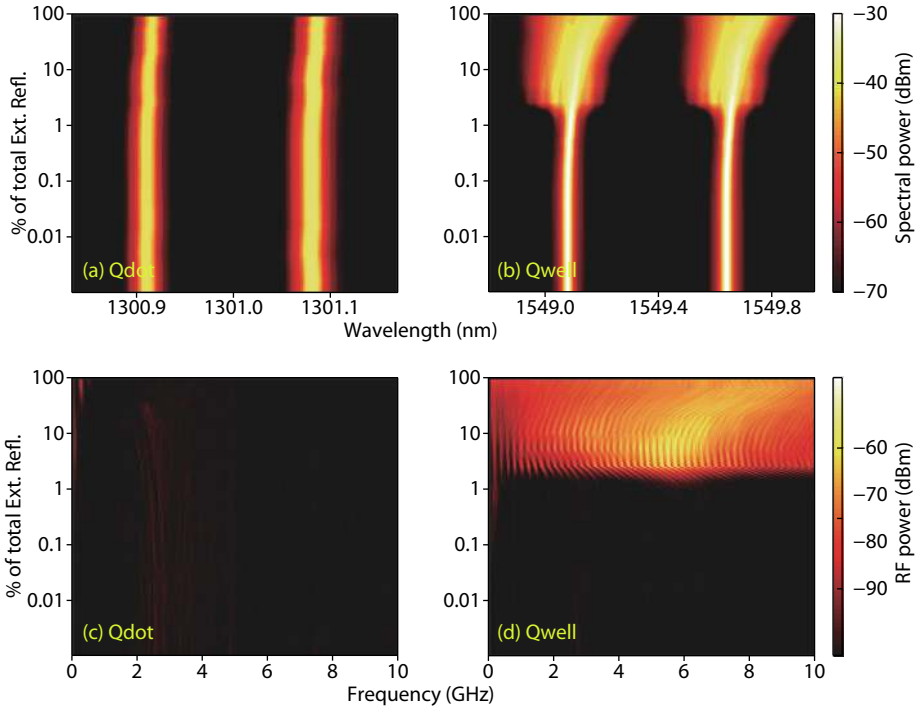

Fig. 11. (Color online) Optical feedback effects on (a, b) the optical power distribution of two cavity modes, and (c, d) on the electrical power distribution. (a) and (c) are for a Si-based Qdot laser (I_{th} = 26.5 mA), (b) and (d) are for a InP-based Qwell laser (I_{th} = 28 mA). (Reproduced from Ref. [63].)

worthwhile to mention that Liao *et al.* reported a Si-based Qdot laser with a low RIN of less than −150 dB/Hz[64]. The strong tolerance of Ge- or Si-based Qdot lasers to the optical feedback can enable the isolator-free operation in PICs on the silicon platform, which is very desirable for practical applications because fabrication of isolators on Si is technically challenging and costive[43, 61, 63, 65].

5. Direct modulation response

For short-reach optical links such as PICs and data centers, direct modulation scheme is more desirable than external modulation one, because the frequency chirp of the laser source does not affect a lot the signal quality in short distance. 1.3 μm InAs/GaAs Qdot lasers have shown record small-signal modulation bandwidth of 13 GHz[66], and large-signal bit rate of 25 Gbps[67]. Meanwhile, 1.5 μm InAs/InP Qdot laser have shown record small-signal bandwidth of 18 GHz[68], and large-signal bit rate of 35 Gbps[69].

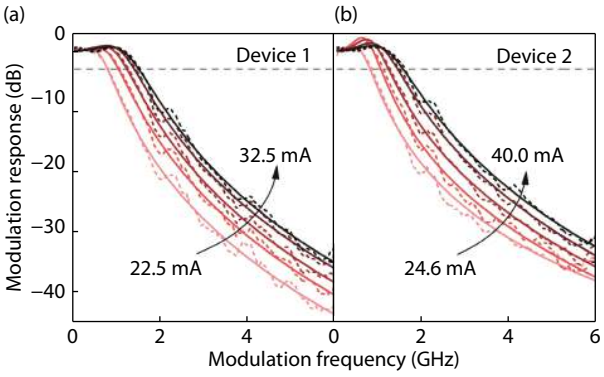

Fig. 12. (Color online) Intensity modulation responses of two Si-based Qdot lasers. The threshold current of device 1 is 18.9 mA, and is 19.1 mA for device 2. The cavity length is 2.5 mm. (Reproduced from Ref. [70].)

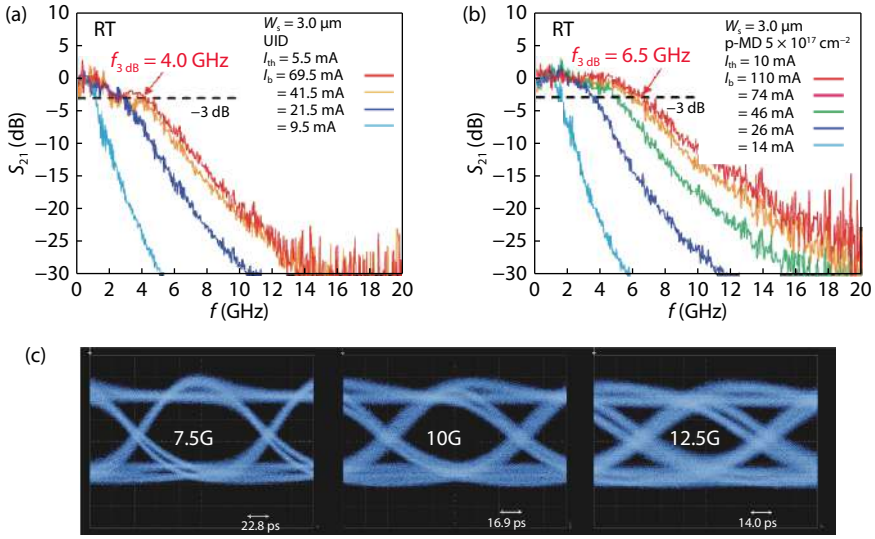

Fig. 13. (Color online) Intensity modulation responses of (a) undoped and (b) p-doped Qdot lasers on Si. (c) Eye diagrams of the p-doped laser, under non-return-to-zero modulation. The cavity length is 0.58 mm. (Reproduced from Ref. [71].)

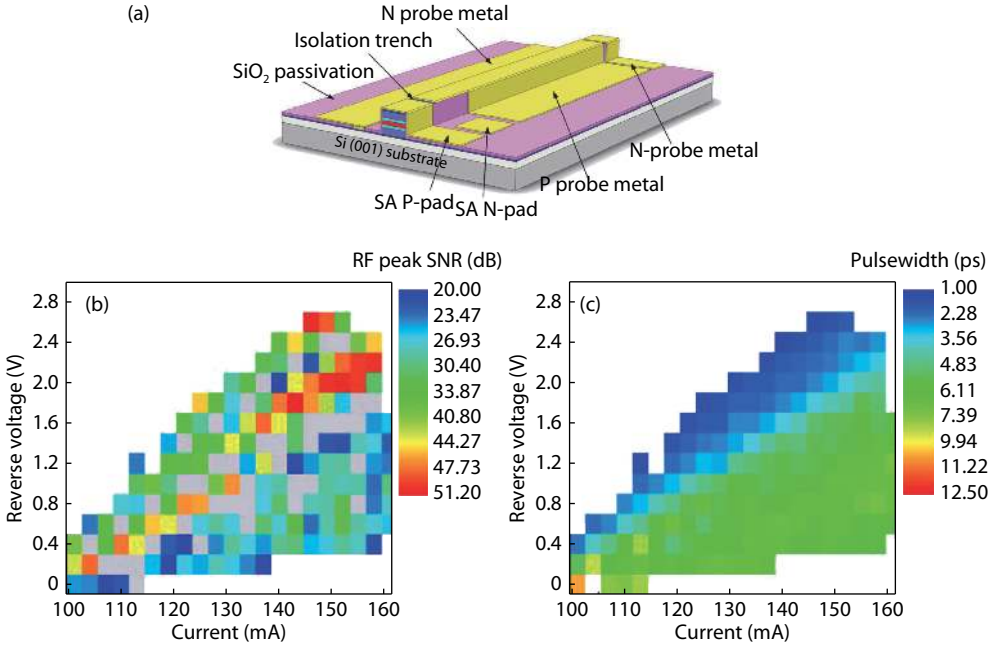

Fig. 14. (Color online) (a) Schematic structure of a mode-locked Qdot laser on Si with a repetition rate of 9.0 GHz. (b) SNR of the fundamental RF peak. (c) Mode-locking pulse width as functions of forward bias current and reverse bias voltage. The threshold current is 90 mA without biasing the absorber section. (Reproduced from Ref. [73].)

Hantschmann *et al.* reported the small-signal modulation response of InAs/GaAs Qdot lasers epitaxially grown on (001) Si with 4° off-cut towards [001] plane[70]. Two nominally identical lasers with a long cavity length of 2.5 mm were tested and the modulation responses are shown in Fig. 12. Both devices show a maximum 3-dB bandwidth of only 1.6 GHz, due to the limitation of long photon lifetime. The extracted *K*-factors for the two devices are 2.4 and 3.7 ns, respectively. Therefore, the resulting maximum intrinsic bandwidths are only 3.7 and 2.4 GHz. In addition, the inverse of the effective carrier lifetime are determined to be 4.0 and 2.0 ns^{-1}, respectively.

Inoue *et al.* reported the direct modulation characteristics of an InAs/GaAs Qdot laser epitaxially grown on on-axis (001)Si[71]. The undoped Si-based laser in Fig. 13(a) exhibits a maximum bandwidth of 4.0 GHz, while the p-doped laser in Fig. 13(b) shows a higher bandwidth of 6.5 GHz. This is because the p-doping in the barriers suppresses the hole depletion, and assists the carrier transport to the dot active region. The *K*-factors for both lasers are 1.3 and 0.92 ns, respectively. This results in maximum intrinsic bandwidths of 6.8 and 9.5 GHz, respectively. Under direct modulation of non-return-to-zero pseudo random bit sequences, the p-doped laser in Fig. 13(c) exhibits extinction ratios of 3.9, 3.7, and 3.3 dB for modulation bit rates of 7.5, 10, and 12.5 Gbps, respectively. In addition, the laser shows no error-floor down to a bit error rate of 1.0×10^{-13}.

6. Mode-locking operation

Mode-locking semiconductor lasers can generate a large

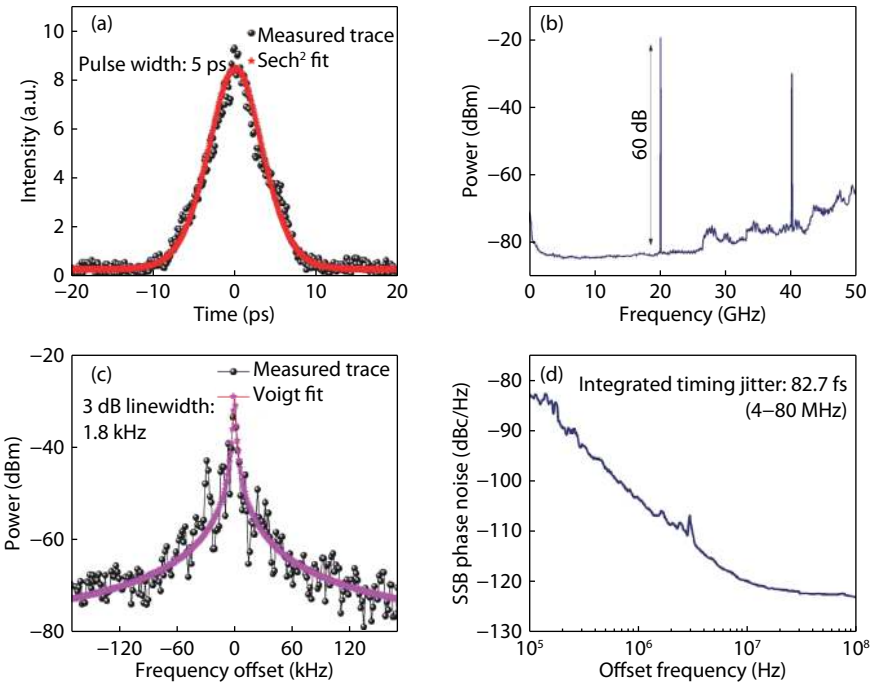

Fig. 15. (Color online) Si-based mode-locked Qdot laser with a repetition rate of 20 GHz. (a) Autocorrelation pulse shape. (b) RF spectrum. (c) RF lineshape. (d) Single-sideband phase noise. The threshold current is 42 mA without biasing the absorber section. (Reproduced from Ref. [79].)

number of coherent longitudinal modes. One mode-locking laser can be used as a multi-channel light source for wavelength division multiplexing communications[72, 73]. In addition, the mode-locked tones can be used for the generation low-noise photonic microwaves through optical heterodyning, which is highly desirable for radio-over-fiber communications[74, 75]. Besides, mode-locked lasers are also valuable for high-speed optical sampling and interchip clock distributions[76, 77]. In comparison with Qwell lasers, Qdot lasers are more desirable for mode locking operation, because of the broad optical spectrum arising from the inhomogeneous broadening effect[72, 78]. Passive mode-locked lasers usually consist of two sections – the gain section and the saturable absorber section, which are electrically isolated. The gain section is forward biased, while the absorber section is reversely biased. The mode locking output is achieved under proper conditions of forward bias current to the gain section associated with reverse bias voltage to the absorber section.

Fig. 14(a) illustrates the schematic structure of an InAs/GaAs Qdot laser epitaxially grown on on-axis (001)Si substrate[71]. The total cavity length is 4.5 mm, and the absorber section length occupies 23%. The full-width of half maximum of the photoluminescence of the gain medium is around 30 meV. Fig. 14(b) presents the evolution of the signal-to-noise (SNR) ratio of the fundamental RF peak at 9.0 GHz, as functions of the forward bias current and the reverse bias voltage. The mode-locking operation is identified when the SNR is larger than 20 dB. It is demonstrated that the mode-locking regime enlarges at a high bias current. The SNR of the fundamental RF peak varies between 20 and 50 dB. On the other hand, the pulse width in Fig. 14(c) varies between 1.0 and 10 ps. A large reverse bias voltage is helpful to narrow the pulse width of the mode-locked laser, which is owing to the reduced absorption recovery time of the absorber section at a high bias voltage.

Fig. 15 shows the characteristics of another mode-locked Qdot laser epitaxially on on-axis (001) Si, which was fabricated in the same group as Fig. 14[79]. The cavity length is 2.05 mm, and the absorption section length occupies 14%, leading to a pulse repetition rate of 20 GHz. The laser employs chirped Qdot design to broaden the width of photoluminescence up to 53 meV. Consequently, the 3-dB optical bandwidth of the mode-locked laser is as high as 6.1 nm, containing 58 longitudinal modes. The laser achieves a narrowest pulse width of 5.0 ps in Fig. 15(a), and the SNR of the fundamental RF peak reaches up to more than 60 dB in Fig. 15(b). In addition, the 3-dB RF linewidth is as narrow as 1.8 kHz in Fig. 15(c), which is comparable to the best mode-locked semiconductor lasers[80, 81]. The timing jitter determined from the single-sideband phase noise (integrating from 4 to 80 MHz) in Fig. 15 (d) results in a record value of 82.7 fs.

In addition to the two-section mode locking scheme, Qdot lasers of one single gain section are widely found to exhibit mode locking as well[82–84]. The physical mechanism for the single-section self-mode locking is still unclear. However, the strong gain compression effect and the large third-order susceptibility in Qdot lasers have been proved to play crucial roles in the self-mode locking behavior[85–87]. Liu *et al.* reported a self-mode locked Qdot laser epitaxially grown on on-axis (001)Si, which exhibited a repetition rate of 31 GHz, associated with a pulse width of 490 fs[84].

7. Future trends

All the Ge- or Si-based Qdot lasers investigated in sections 3–6 are based on Fabry-Perot cavity, which emit on multimodes. However, practical applications in optical communication and in optical computing require single-mode laser sources, which are widely achieved through using the distributed feedback (DFB) gratings. Wang *et al.* have successfully demonstrated DFB Qdot laser arrays on off-cut (001) Si substrate, which showed a high side mode suppression ratio of 50 dB. Besides, the DFB laser arrays cover the full spectral

span of the O band, with a channel spacing of 20 nm[88]. However, there was no report on the spectral linewidth or the phase noise of the DFB lasers. The spectral linewidth of Qdot lasers on GaAs or InP is usually several hundred kilohertz, which is one order of magnitude smaller than typical Qwell lasers[89–94]. The record linewidth of an InAs/InP Qdot DFB laser reaches as low as 50 kHz[94]. Continuous-wave DFB laser is ready for external modulation, in combination with optical modulators. However, directly-modulated DFB Qdot lasers on Si are yet to develop in future work. For data transmission speed up to 10 Gbps, isolator-free Qdot laser with direct modulation may become the dominate solution for PICs on Si in the future. In contrast, external modulation scheme may be still required for speed more than 25 Gbps, due to the bandwidth limitation of Qdot lasers.

Most Qdot lasers epitaxially grown on Si are operated in the O band, while C band laser emission is required for long-haul communication. However, it is more challenging to directly grown 1.5 μm InAs/InP Qdot lasers on Si than 1.3 μm InAs/GaAs Qdot lasers, because the lattice mismatch between InP and Si is as large as about 8%, twice the mismatch between GaAs and Si. This problem is circumvented by using V-grooved Si substrate, which traps most twined stacking faults in Si[95, 96]. However, the defect density at the interface of the InP buffer layer is still as high as 10^9–10^{10} cm^{-2}[96]. In spite of these difficulties, Zhu *et al.* successfully demonstrated InAs/InP Qdot laser epitaxially grown on (001) Si, with pulsed current pumping[97]. The dynamical characteristics of InAs/InP Qdot lasers on Si require investigation in future work, as those discussed in Sections 3–6.

Fabry-Perot or DFB lasers typically have a footprint in the millimeter range. In order to reduce the footprint of laser sources on Si down to the micrometer range, Si-based microdisk lasers and micro-ring lasers have been developed[98–103]. Particularly, Wan *et al.* demonstrated a Qdot micro-ring laser on (001) Si with an ultralow threshold of 0.6 mA[101]. An alternative approach for reducing the footprint is to employ the nano-ridge structure[104–107]. Using this structure, Han *et al.* successfully demonstrated InP/InGaAs nano-ridge lasers on (001) Si with optical pumping. Interestingly, the lasing wavelength is widely tunable ranging from O band up to the C band, through changing the excitation level and the nano-ridge length.

8. Conclusion

In summary, this work systematically discussed recent progresses on the dynamical characteristics of Qdot lasers epitaxially grown on Ge or Si, including the LBF, the RIN and the FN, the modulation response, the sensitivity to optical feedback, and mode-locked performances. Although there is high density of epitaxial defects, some dynamical performances of Ge- or Si-based Qdot lasers are becoming comparable to those of GaAs-based ones. Particularly, these lasers are highly tolerant to optical feedback, owing to the defect-enhanced damping factor. However, it is still highly desirable to further reduce the defect density for further improving both static and dynamic performances. Once Qdot lasers are properly integrated on the Si platform, the next challenging task in future work is to figure out approaches to efficiently couple the laser light into optical waveguides, which connect a large variety of photonic and optoelectronic devices in PICs.

Acknowledgments

This work is supported by National Natural Science Foundation of China (No. 61804095), and by Shanghai Pujiang Program (No. 17PJ1406500).

References

[1] Soref R. The past, present, and future of silicon photonics. IEEE J Sel Top Quantum Electron, 2006, 12(6), 1678
[2] Lin X, Riveson Y, Yardimci N T, et al. All-optical machine learning using diffractive deep neural networks. Science, 2018, 361(6406), 1004
[3] Cardenas J, Poitras C B, Robinson J T, et al. Low loss etchless silicon photonic waveguides. Opt Express, 2009, 17(6), 4752
[4] Vivien L, Osmond J, Fédéli J M, et al. 42 GHz p.i.n germanium photodetector integrated in a silicon-on-insulator waveguide. Opt Express, 2009, 17(8), 6252
[5] Reed G T, Mashanovich G, Gardes F Y, et al. Silicon optical modulators. Nat Photon, 2010, 4(8), 518
[6] Liang D, Bowers J E. Recent progress in lasers on silicon. Nat Photon, 2010, 4(8), 511
[7] Alcotte R, Martin M, Moeyaert J, et al. Epitaxial growth of antiphase boundary free GaAs layer on 300 mm Si (001) substrate by metalorganic chemical vapour deposition with high mobility. APL Mater, 2016, 4(4), 046101
[8] Liu A Y, Herrick R W, Ueda O, et al. Reliability of InAs/GaAs quantum dot lasers epitaxially grown on silicon. IEEE J Sel Top Quantum Electron, 2015, 21(6), 690
[9] Tanabe K, Rae T, Watanabe K, et al. High-temperature 1.3 μm InAs/GaAs quantum dot lasers on Si substrates fabricated by wafer bonding. Appl Phys Express, 2013, 6(8), 082703
[10] Urino Y, Hatori N, Mizutani K, et al. First demonstration of athermal silicon optical interposers with quantum dot lasers operating up to 125 °C. J Lightw Technol, 2015, 33(6), 1223
[11] Uvin S, Kumari S, Groote A D, et al. 1.3 μm InAs/GaAs quantum dot DFB laser integrated on a Si waveguide circuit by means of adhesive die-to-wafer bonding. Opt Express, 2018, 26(14), 18302
[12] Liu H, Wang T, Jiang Q, et al. Long-wavelength InAs/GaAs quantum-dot laser diode monolithically grown on Ge substrate. Nat Photon, 2011, 5(7), 416
[13] Norman J C, Jung D, Wan Y, et al. Perspective: The future of quantum dot photonic integrated circuits. APL Photonics, 2018, 3(3), 030901
[14] Jung D, Herrick R, Norman J, et al. Impact of threading dislocation density on the lifetime of InAs quantum dot lasers on Si. Appl Phys Lett, 2018, 112(15), 153507
[15] O'Brien D, Hegarty S P, Huyet G, et al. Feedback sensitivity of 1.3 μm InAs/GaAs quantum dot lasers. Electron Lett, 2003, 39(25), 1819
[16] Deppe D G, Shavritranuruk K, Ozgur G, et al. Quantum dot laser diode with low threshold and low internal loss. Electron Lett, 2009, 45(1), 54
[17] Sugawara M, Usami M. Quantum dot devices handling the heat. Nat Photon, 2009, 3(1), 30
[18] Lee A, Jiang Q, Tang M, et al. Continuous-wave InAs/GaAs quantum-dot laser diodes monolithically grown on Si substrate with low threshold current densities. Opt Express, 2012, 20(20), 22181
[19] Chen S, Li W, Wu J, et al. Electrically pumped continuous-wave III–V quantum dot lasers on silicon. Nat Photon, 2016, 10(10), 307
[20] Liu A Y, Peters J, Huang X, et al. Electrically pumped continuous-wave 1.3 μm quantum-dot lasers epitaxially grown on on-axis (001) GaP/Si. Opt Lett, 2017, 42(2), 338

[21] Tischler M A, Katsuyama T, El-Masry N A, et al. Defect reduction in GaAs epitaxial layers using a GaAsP–InGaAs strained-layer superlattice. Appl Phys Lett, 1985, 46(3), 294

[22] Liu A Y, Zhang C, Norman J, et al. High performance continuous wave 1.3 μm quantum dot lasers on silicon. Appl Phys Lett, 2014, 104(4), 041104

[23] Lee A D, Jiang Q, Tang M, et al. InAs/GaAs quantum-dot lasers monolithically grown on Si, Ge, and Ge-on-Si substrates. IEEE J Sel Top Quantum Electron, 2013, 19(4), 1901107

[24] Liu A Y, Srinivasan S, Norman J, et al. Quantum dot lasers for silicon photonics. Photon Res, 2015, 3(5), B1

[25] Norman J C, Jung D, Zhang Z, et al. A review of high-performance quantum dot lasers on silicon. IEEE J Quantum Electron, 2019, 55(2), 1

[26] Wang C, Zhuang J P, Grillot F, et al. Contribution of off-resonant states to the phase noise of quantum dot lasers. Opt Express, 2016, 24(26), 29872

[27] Sears K, Buda M, Tan H, et al. Modeling and characterization of InAs/GaAs quantum dot lasers grown using metal organic chemical vapor deposition. J Appl Phys, 2007, 101(1), 013112

[28] Bimberg D, Grundmann M, Ledentsov N N. Quantum dot heterostructures. Hoboken: John Wiley & Sons, 1999

[29] Linder K K, Phillips J, Oasaimeh O, et al. Self-organized $In_{0.4}Ga_{0.6}As$ quantum-dot lasers grown on Si substrates. Appl Phys Lett, 1999, 74(10), 1355

[30] Coldren L A, Corzine S W, Mashanovitch M L. Diode lasers and photonic integrated circuits. Hoboken: John Wiley & Sons, 2012

[31] Osinski M, Buus J. Linewidth broadening factor in semiconductor lasers–An overview. IEEE J Quantum Electron, 1987, 23(1), 9

[32] Hwang S K, Liang D H. Effects of linewidth enhancement factor on period-one oscillations of optically injected semiconductor lasers. Appl Phys Lett, 2006, 89(6), 061120

[33] Melnik S, Huyet G. The linewidth enhancement factor α of quantum dot semiconductor lasers. Opt Express, 2006, 14(7), 2950

[34] Gioannini M, Montrosset I. Numerical analysis of the frequency chirp in quantum-dot semiconductor lasers. IEEE J Quantum Electron, 2007, 43(10), 941

[35] Globisch B, Otto C, Scholl E, et al. Influence of carrier lifetimes on the dynamical behavior of quantum-dot lasers subject to optical feedback. Phys Rev E, 2012, 86(4), 046201

[36] Bimberg D, Kirstaedter N, Ledentsov N N, et al. InGaAs–GaAs quantum-dot lasers. IEEE J Sel Top Quantum Electron, 1997, 3(2), 196

[37] Newell T C, Bossert D J, Stintz A, et al. Gain and linewidth enhancement factor in InAs quantum-dot laser diodes. IEEE Photon Technol Lett, 1999, 11(12), 1527

[38] Dagens B, Markus A, Chen J X, et al. Giant linewidth enhancement factor and purely frequency modulated emission from quantum dot laser. Electron Lett, 2005, 41(6), 323

[39] Mi Z, Bhattacharya P. DC and dynamic characteristics of P-doped and tunnel injection 1.65-μm InAs quantum-dash lasers grown on InP (001). IEEE J Quantum Electron, 2006, 42(12), 1224

[40] Martinez A, Merghem K, Bouchoule S, et al. Dynamic properties of InAs/InP (311)B quantum dot Fabry-Perot lasers emitting at 1.52 μm. Appl Phys Lett, 2008, 93(2), 021101

[41] Bhowmick S, Baten M Z, Frost T, et al. High performance InAs/$In_{0.53}Ga_{0.23}Al_{0.24}As$/InP quantum dot 1.55 μm tunnel injection laser. IEEE J Quantum Electron, 2014, 50(1), 7

[42] Gioannini M, Sevega A, Montrosset I. Simulations of differential gain and linewidth enhancement factor of quantum dot semiconductor lasers. Opt Quantum Electron, 2006, 38(4–6), 381

[43] Zhou Y G, Zhao X Y, Cao C F, et al. High optical feedback tolerance of InAs/GaAs quantum dot lasers on germanium. Opt Express, 2018, 26(21), 28131

[44] Ahmed M, Yamada M, Saito M. Numerical modeling of intensity and phase noise in semiconductor lasers. IEEE J Quantum Electron, 2001, 37(12), 1600

[45] Fronen R J, Vandamme L K J. Low-frequency intensity noise in semiconductor lasers. IEEE J Quantum Electron, 1988, 24(5), 724

[46] Capua A, Rozenfeld L, Mikhelashvili V, et al. Direct correlation between a highly damped modulation response and ultra low relative intensity noise in an InAs/GaAs quantum dot laser. Opt Express, 2007, 15(9), 5388

[47] Duan J, Wang X G, Zhou Y G, et al. Carrier-noise-enhanced relative intensity noise of quantum dot lasers. IEEE J Quantum Electron, 2018, 54(6), 1

[48] Ohtsubo J. Semiconductor lasers: Stability, Instability and Chaos. New York: Springer, 2012

[49] O'Brien D, Hegarty S P, Huyet G, et al. Sensitivity of quantum-dot semiconductor lasers to optical feedback. Opt Lett, 2004, 29(10), 1072

[50] Binder J O, Cormack G D. Mode selection and stability of a semiconductor laser with weak optical feedback. IEEE J Quantum Electron, 1989, 25(11), 2255

[51] Helms J, Petermann K. A simple analytic expression for the stable operation range of laser diode with optical feedback. IEEE J Quantum Electron, 1990, 26(5), 833

[52] Tromborg B, Mork J. Nonlinear injection locking dynamics and the onset of coherence collapse in external cavity lasers. IEEE J Quantum Electron, 1990, 26(4), 642

[53] Wang C, Schires K, Osinski M, et al. Thermally insensitive determination of the linewidth broadening factor in nanostructured semiconductor lasers using optical injection locking. Sci Rep, 2016, 6, 27825

[54] Zhou Y G, Duan J, Huang H, et al. Intensity noise and pulse oscillation of an InAs/GaAs quantum dot laser on germanium. IEEE J Sel Top Quantum Electron, 2019, 25(6), 1

[55] Duan J, Huang H, Jung D, et al. Semiconductor quantum dot lasers epitaxially grown on silicon with low linewidth enhancement factor. Appl Phys Lett, 2018, 112(25), 251111

[56] Jung D, Norman J, Kennedy M J, et al. High efficiency low threshold current 1.3 μm InAs quantum dot lasers on on-axis (001) GaP/Si. Appl Phys Lett, 2017, 111(12), 122107

[57] Jungho K, Hui S, Minin S, et al. Comparison of linewidth enhancement factor between p-doped and undoped quantum-dot lasers. IEEE Photon Technol Lett, 2006, 18(9), 1022

[58] Zhou Y G, Zhou C, Cao C F, et al. Relative intensity noise of InAs quantum dot lasers epitaxially grown on Ge. Opt Express, 2017, 25(23), 28817

[59] Feiste U. Optimization of modulation bandwidth in DBR lasers with detuned bragg reflectors. IEEE J Quantum Electron, 1998, 34(12), 2371

[60] Laakso A, Dumitrescu M. Modified rate equation model including the photon-photon resonance. Opt Quantum Electron, 2011, 42(11–13), 785

[61] Liu A Y, Komljenovic T, Davenport M L, et al. Reflection sensitivity of 1.3 μm quantum dot lasers epitaxially grown on silicon. Opt Express, 2017, 25(9), 9535

[62] Schunk N, Petermann K. Numerical analysis of the feedback regimes for a single-mode semiconductor laser with external feedback. IEEE J Quantum Electron, 1988, 24(7), 1242

[63] Duan J, Huang H, Dong B, et al. 1.3-μm reflection insensitive InAs/GaAs quantum dot lasers directly grown on silicon. IEEE Photon Technol Lett, 2019, 31(5), 345

[64] Liao M, Chen S, Liu Z, et al. Low-noise 1.3 μm InAs/GaAs quantum dot laser monolithically grown on silicon. Photon Res, 2018, 6(11), 1062

[65] Huang H, Duan J, Jung D, et al. Analysis of the optical feedback dynamics in InAs/GaAs quantum dot lasers directly grown on silicon. J Opt Soc Am B, 2018, 35(11), 2780

[66] Kageyama T, Vo Q H, Watanabe K, et al. Large modulation band-

width (13.1 GHz) of 1.3 μm-range quantum dot lasers with high dot density and thin barrier layer. Compound Semiconductor Week, 2016, MoC3-4

[67] Ishida M, Matsuda M, Tanaka Y, et al. Temperature-stable 25-Gbps direct-modulation in 1.3-μm InAs/GaAs quantum dot lasers. Conference on Lasers and Electro-Optics, 2012, CM1I.2

[68] Abdollahinia A, Banyoudeh S, Rippien A, et al. Temperature stability of static and dynamic properties of 1.55 μm quantum dot lasers. Opt Express, 2018, 26(5), 6056

[69] Banyoudeh S, Abdollahinia A, Eyal O, et al. Temperature-insensitive high-speed directly modulated 1.55-μm quantum dot lasers. IEEE Photon Technol Lett, 2016, 28(21), 2451

[70] Hantschmann C, Vasilev P P, Wonfor A, et al. Understanding the bandwidth limitations in monolithic 1.3 μm InAs/GaAs quantum dot lasers on silicon. J Lightw Technol, 2019, 37(3), 949

[71] Inoue D, Jung D, Norman J, et al. Directly modulated 1.3 μm quantum dot lasers epitaxially grown on silicon. Opt Express, 2018, 26(6), 7022

[72] Thompson M G, Rae A R, Mo X, et al. InGaAs quantum-dot mode-locked laser diodes. IEEE J Sel Top Quantum Electron, 2009, 15(3), 661

[73] Liu S, Norman J C, Jung D, et al. Monolithic 9 GHz passively mode locked quantum dot lasers directly grown on on-axis (001) Si. Appl Phys Lett, 2018, 113(4), 041108

[74] Simonis G J, Purchase K G. Optical generation, distribution, and control of microwaves using laser heterodyne. IEEE Trans Microwave Theory Tech, 1990, 38(5), 667

[75] Stöhr A, Akrout A, Buß R, et al. 60 GHz radio-over-fiber technologies for broadband wireless services. J Opt Netw, 2009, 8(5), 471

[76] Delfyett P J, Hartman D H, Ahmad S Z. Optical clock distribution using a mode-locked semiconductor laser diode system. J Lightw Technol, 1991, 9(12), 1646

[77] Ohno T, Sato K, Iga R, et al. Recovery of 160 GHz optical clock from 160 Gbit/s data stream using mode locked laser diode. Electron Lett, 2004, 40(4), 265

[78] Rafailov E U, Cataluna M A, Sibbett W. Mode-locked quantum-dot lasers. Nature Photon, 2007, 1(7), 395

[79] Liu S, Wu X, Jung D, et al. High-channel-count 20 GHz passively mode-locked quantum dot laser directly grown on Si with 41 Tbit/s transmission capacity. Optica, 2019, 6(2), 128

[80] Carpintero G, Thompson M G, Penty R V, et al. Low noise performance of passively mode-locked 10-GHz quantum-dot laser diode. IEEE Photon Technol Lett, 2009, 21(6), 389

[81] Davenport M L, Liu S, Bowers J E. Integrated heterogeneous silicon/III–V mode-locked lasers. Photon Res, 2018, 6(5), 468

[82] Renaudier J, Brenot R, Dagens B, et al. 45 GHz self-pulsation with narrow linewidth in quantum dot Fabry-Perot semiconductor lasers at 1.5 μm. Electron Lett, 2005, 41(18), 1007

[83] Liu J, Liu Z, Raymond S, et al. Dual-wavelength 92.5 GHz self-mode-locked InP-based quantum dot laser. Opt Lett, 2008, 33(15), 1702

[84] Liu S, Jung D, Norman J C, et al. 490 fs pulse generation from passively mode-locked single section quantum dot laser directly grown on on-axis GaP/Si. Electron Lett, 2018, 54(7), 432

[85] Rossetti M, Tianhong X, Bardella P, et al. Impact of gain saturation on passive mode locking regimes in quantum dot lasers with straight and tapered waveguides. IEEE J Quantum Electron, 2011, 47(11), 1404

[86] Rossetti M, Bardella P, Montrosset I. Time-domain travelling-wave model for quantum dot passively mode-locked lasers. IEEE J Quantum Electron, 2011, 47(2), 139

[87] Bardella P, Columbo L L, Gioannini M. Self-generation of optical frequency comb in single section quantum dot Fabry-Perot lasers: a theoretical study. Opt Express, 2017, 25(21), 26234

[88] Wang Y, Chen S, Yu Y, et al. Monolithic quantum-dot distributed feedback laser array on silicon. Optica, 2018, 5(5), 528

[89] Su H, Lester L F. Dynamic properties of quantum dot distributed feedback lasers: high speed, linewidth and chirp. J Phys D, 2005, 38(13), 2112

[90] Lu Z G, Poole P J, Liu J R, et al. High-performance 1.52 μm InAs/InP quantum dot distributed feedback laser. Electron Lett, 2011, 47(14), 818

[91] Becker A, Sichkovskyi V, Bjelica M, et al. Narrow-linewidth 1.5-μm quantum dot distributed feedback lasers. Proc SPIE, 2016, 97670Q

[92] Septon T, Gosh S, Becker A, et al. Spectral characteristics of narrow linewidth InAs/InP quantum dot distributed feedback lasers. 26th International Semiconductor Laser Conference, 2018, TuD4

[93] Duan J, Huang H, Lu Z G, et al. Narrow spectral linewidth in InAs/InP quantum dot distributed feedback lasers. Appl Phys Lett, 2018, 112(12), 121102

[94] Septon T, Gosh S, Becker A, et al. Narrow linewidth InAs/InP quantum dot DFB laser. Optical Fiber Communication Conference, 2019, W3A.8

[95] Wan Y, Li Q, Geng Y, et al. InAs/GaAs quantum dots on GaAs-on-V-grooved-Si substrate with high optical quality in the 1.3 μm band. Appl Phys Lett, 2015, 107(8), 081106

[96] Li Q, Ng K W, Lau K M. Growing antiphase-domain-free GaAs thin films out of highly ordered planar nanowire arrays on exact (001) silicon. Appl Phys Lett, 2015, 106(7), 072105

[97] Zhu S, Shi B, Li Q, et al. 1.5 μm quantum-dot diode lasers directly grown on CMOS-standard (001) silicon. Appl Phys Lett, 2018, 113(22), 221103

[98] Wan Y, Li Q, Liu A Y, et al. Sub-wavelength InAs quantum dot micro-disk lasers epitaxially grown on exact Si (001) substrates. Appl Phys Lett, 2016, 108(22), 221101

[99] Wan Y, Li Q, Liu A Y, et al. Optically pumped 1.3 μm room-temperature InAs quantum-dot micro-disk lasers directly grown on (001) silicon. Opt Lett, 2016, 41(7), 1664

[100] Wan Y, Jung D, Norman J, et al. O-band electrically injected quantum dot micro-ring lasers on on-axis (001) GaP/Si and V-groove Si. Opt Express, 2017, 25(22), 26853

[101] Wan Y, Norman J, Li Q, et al. 1.3 μm submilliamp threshold quantum dot micro-lasers on Si. Optica, 2017, 4(8), 940

[102] Shi B, Zhu S, Li Q, et al. 1.55 μm room-temperature lasing from subwavelength quantum-dot microdisks directly grown on (001) Si. Appl Phys Lett, 2017, 110(12), 121109

[103] Shi B, Zhu S, Li Q, et al. Continuous-wave optically pumped 1.55 μm InAs/InAlGaAs quantum dot microdisk lasers epitaxially grown on silicon. ACS Photonics, 2017, 4(2), 204

[104] Han Y, Li Q, Zhu S, et al. Continuous-wave lasing from InP/InGaAs nanoridges at telecommunication wavelengths. Appl Phys Lett, 2017, 111(21), 212101

[105] Han Y, Ng W K, Ma C, et al. Room-temperature InP/InGaAs nanoridge lasers grown on Si and emitting at telecom bands. Optica, 2018, 5(8), 918

[106] Han Y, Li Q, Ng K W, et al. InGaAs/InP quantum wires grown on silicon with adjustable emission wavelength at telecom bands. Nanotechnology, 2018, 29(22), 225601

[107] Han Y, Ng W K, Xue Y, et al. Telecom InP/InGaAs nanolaser array directly grown on (001) silicon-on-insulator. Opt Lett, 2019, 44(4), 767